Magnetic response of nanoscale left-handed metamaterials

R. S. Penciu,[1] M. Kafesaki,[1,2,*] Th. Koschny,[1,3] E. N. Economou,[1,4] and C. M. Soukoulis[1,2,3]
[1]*Institute of Electronic Structure and Laser (IESL), Foundation for Research and Technology Hellas (FORTH), P.O. Box 1385, 71110 Heraklion, Crete, Greece*
[2]*Department of Materials Science and Technology, University of Crete, 71003 Heraklion, Greece*
[3]*Ames Laboratory and Department of Physics and Astronomy, Iowa State University, Ames, Iowa 50011, USA*
[4]*Department of Physics, University of Crete, 71003 Heraklion, Greece*
(Received 7 January 2010; revised manuscript received 31 March 2010; published 11 June 2010)

Using detailed simulations we investigate the magnetic response of metamaterials consisting of pairs of parallel slabs or combinations of slabs with wires (including the fishnet design) as the length scale of the structures is reduced from millimeter to nanometer. We observe the expected saturation of the magnetic-resonance frequency when the structure length scale goes to the submicron regime, as well as weakening of the effective permeability resonance and reduction in the spectral width of the negative permeability region. All these results are explained by using an equivalent resistor-inductor-capacitor circuit model, taking into account the current-connected kinetic energy of the electrons inside the metallic parts through an equivalent inductance, added to the magnetic field inductance in the unit cell. Using this model we derive simple optimization rules for achieving optical negative permeability metamaterials with improved performance. Finally, we analyze the magnetic response of the fishnet design and we explain its superior performance regarding the high attainable magnetic-resonance frequency, as well as its poor performance regarding the width of the negative permeability region.

DOI: 10.1103/PhysRevB.81.235111 PACS number(s): 41.20.Jb, 42.70.Qs, 81.05.Xj, 78.67.Pt

I. INTRODUCTION

Left-handed metamaterials (LHMs), i.e., artificial composite structures with overlapping negative permittivity and permeability frequency bands giving rise to negative index of refraction,[1–4] have recently attracted an exponentially increasing attention. The main reason behind this attention is the peculiar physical phenomena associated with those materials (negative refraction, opposite phase and energy velocity, reversed Doppler effect, etc.), which result in different capabilities for the manipulation of electromagnetic waves. One such important capability of LHMs is superlensing,[5] i.e., the ability to offer subwavelength resolution imaging; this can have important implications in many scientific, technological, and everyday life areas, such as imaging, microscopy, lithography, ultracompact data storage, etc.

Since the demonstration of the first LHM,[6] in 2000, operating in the microwave regime, many LH structures have been created,[7–13] and important efforts for the better understanding and the optimization of those structures have taken place. Among the various efforts within the LHM research, a large part has been devoted to the extension of the frequency of operation of LHMs from the microwaves to the optical regime, where superlensing-based applications can find an important ground for their manifestation. These efforts led to metamaterials with negative permeability operating in the few terahertz regime as early as 2004,[14,15] which soon were followed by the first structures of negative permeability and/or negative index of refraction in the telecommunications regime[16] and more recently in the lower visible regime.[17] (For reviews of the existing research efforts on infrared (IR) and optical metamaterials see Refs. 18–20.)

While the first and most of the current microwave LHMs are systems made of split-ring resonators[21] (SRRs, i.e., interrupted metallic rings, giving rise to resonant looplike currents and thus to a resonant permeability involving negative permeability values) and continuous wires (leading to the negative permittivity response[22]), in most of today's high-frequency LHMs the SRRs have been replaced by pairs of slabs (or stripes or wires)[23–26]—see Fig. 1(a). Like the SRR, the slab pair also behaves as a resonant magnetic-moment element, where the magnetic moment is created by resonant currents, antiparallel in the two slabs of the pair, forming a looplike current. In most of the experimentally realized optical slab-pair&wire structures the slabs are as wide as the corresponding unit-cell side and are physically connected with the wires, leading to a design known as fishnet[27–31] [see Fig. 1(d)]. The fishnet design was able to give the highest in frequency LHMs to date.[17,32,33]

The main reason behind the replacement of SRR by the slab pair for the high-frequency metamaterials, apart from the slab-pair simplicity in fabrication (which is also a crucial parameter), is its ability to exhibit a negative permeability response for incidence normal to the plane of the pair; this makes possible the demonstration of the negative permeability response with just a monolayer of slab pairs. Indeed, up to now most of the demonstrated "magnetic" metamaterials (i.e., materials with resonant and negative permeability) and LHMs are single layers while only a few multilayer samples have been fabricated.[15,34–36] (Note that in the optical regime what is difficult to achieve is the negative permeability component of a LHM, since the negative permittivity response can be easily obtained using metals; that is why most of the existing efforts to go to optical LHMs start from attempts to achieve structures with only negative permeability.)

Since many of the existing attempts to create high-frequency magnetic metamaterials and LHMs are based on the scaling down of known microwave designs, there are already efforts trying to determine the possibilities and the

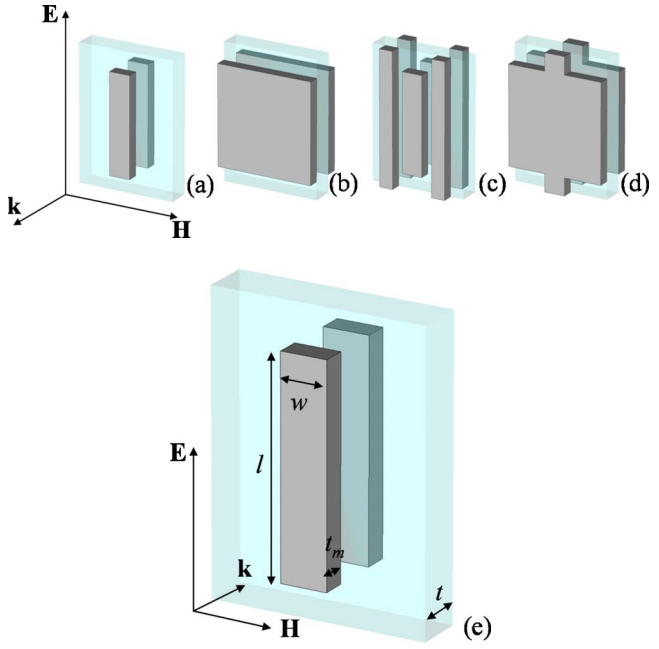

FIG. 1. (Color online) The unit cell of the four designs studied. (a) Narrow-slab-pair system; (b) wide-slab-pair system; (c) slabs&wires system; and (d) fishnet design. Panel (e) is a magnification of panel (a) where the structure parameters appearing in the structure simulations are shown. The parameters of the pair are given as a function of the scale parameter $a=a_{\mathbf{k}}$ (lattice constant along propagation direction; equal to the system thickness): lattice constants $a_{\mathbf{E}}=2.97a_{\mathbf{k}}$, $a_{\mathbf{H}}=2.19a_{\mathbf{k}}$, slab length $l=2.19a_{\mathbf{k}}$, slab width $w=0.47a_{\mathbf{k}}$, thickness of the metal $t_m=0.25a_{\mathbf{k}}$, and thickness of the substrate $t=0.5a_{\mathbf{k}}$. For the fishnet design (d) the width of the slabs is equal to the corresponding unit-cell side ($a_{\mathbf{H}}$) while the width of the "necks" (continuous metallic parts joining the slabs along **E** direction) is $w_n=0.469a_{\mathbf{k}}$. The dielectric spacer separating the metallic pairs has been considered as glass (with relative permittivity $\varepsilon_b=2.14$) while for the metal plasma frequency and damping factor the aluminum parameters have been employed.

limitations of this scaling approach.[37–40] (Note that the properties of the metals, which are involved in most of today's metamaterials, are drastically different in the optical regime compared to microwaves—there, metals behave almost as perfect conductors.) Most of those attempts concern SRR systems and they have led to two important conclusion:[37,41,42]

(a) By scaling down a SRR, the frequency of its resonant magnetic response does not continuously increase but after some length scale it saturates to a constant value. This value was found to be dependent on the SRR geometry employed, and with proper modifications of this geometry (e.g., adding gaps in the SRR) it could go up to a small fraction (e.g., 20%) of the plasma frequency, i.e., to the middle visible range. The saturation response of the magnetic-resonance frequency was explained by taking into account the contribution of the kinetic energy of the electrons associated with the current inside the SRR ring to the magnetic energy created by the loop current (or, equivalently, taking into account the dispersive response of the metal to the conductivity).

(b) The magnetic permeability resonance becomes weaker and weaker by going to smaller length-scale SRR systems and below some length scale it ceases to reach negative values. This weakening of the permeability was attributed to the kinetic energy of the electrons (giving rise to saturation) in combination with the increased resistive losses in the metal as one goes to higher frequencies; these losses are strengthened by the resonant response, implying long-time interaction of the wave with the metallic structures.

Although the existing studies are very revealing concerning the high-frequency response of magnetic metamaterials, they examine the influence of the kinetic energy (or the dispersive response of the metals) only in the magnetic-resonance frequency and not to other, equally important features of the resonant magnetic response, such as resonance shape and damping factor, total losses, and spectral width of the negative permeability band; moreover, they did not clarify the role of the ohmic losses in the saturation of the magnetic-resonance frequency. Finally, the role of the various geometrical parameters in the high-frequency response of metamaterials still remains to be determined, so as to identify the dominant parameters for this response and to define optimization rules for high-frequency metamaterials. (Note that today's IR and optical negative index metamaterials suffer from very high losses, which make these structures nonfunctional. Structure optimization so as to minimize the overlap of the field with the metallic components can be proved to be a very efficient way for the reduction in the total losses.)

In this paper we attempt to study all the above issues. We will restrict ourselves to systems based on pairs of slabs, alone, or in combination with continuous wires; this is mainly due to the fact that slab-pair-based systems offer an easy experimental demonstration of negative permeability or negative index response and, moreover, have been proven up to now the most promising systems for the achievement of high-frequency negative permeability and negative index metamaterials.[18,19] The structures discussed here are shown in Fig. 1. We will attempt to analyze the high-frequency magnetic response of these structures, to compare their performance, and to propose optimization rules for them. For that we examine in detail the scaling behavior of the magnetic-resonance frequency and the magnetic permeability as the structures are scaled down from millimeter to nanometer scale.

The basic idea that we will use to reproduce and understand the small length-scale (high-frequency) behavior of our structures is the consideration of the kinetic energy of the current-carrying electrons.[37] This kinetic energy, as being proportional to the square of the velocity (and thus of the frequency, just like the magnetic energy), is added to the magnetic energy of the structures and for small length scales dominates the magnetic metamaterials response. The consideration of this kinetic energy is done here through an equivalent "kinetic" inductance[37,43] (or electrons' inductance), added to the magnetic field inductance in an effective resistor-inductor-capacitor (RLC) description of the artificial magnetic structures.

Specifically, the paper is organized as follows: in Sec. II we present the "high-frequency" response of our structures, as revealed by numerical simulations concerning the magnetic-resonance frequency, the form of the magnetic per-

meability resonance, the bandwidth of the negative permeability band, and the losses. The wave propagation characteristics in these structures are analyzed and explained in Sec. III, using an effective RLC description of the structures and taking into account the dispersive behavior of the metals through the kinetic metal inductance. Based on the results and analysis of Secs. II and III, in Sec. IV we present basic optimization rules for the achievement of high-frequency magnetic metamaterials and left-handed materials with improved performance. There we discuss also the fishnet design, which has been proven up to now to be the optimum design for achievement of optical negative index materials. Finally, in Sec. V we show that the simple RLC circuit model does not only have qualitative power but it can also be used to give quantitative results if plugged with accurate relations for the capacitance and the inductance of the system.

II. NUMERICAL SIMULATIONS

In this section we present calculation results concerning the scaling of the magnetic-resonance frequency and the magnetic permeability of the structures shown in Fig. 1. The geometrical parameters used in the simulations are those mentioned in Fig. 1; for the permittivity of the metal, the Drude dispersion model has been employed, i.e., $\varepsilon=\varepsilon_0[\varepsilon^{(0)}-\omega_p^2/(\omega^2+i\omega\gamma_m)]$, with the parameters of the aluminum (plasma frequency $\omega_p=22.43\times10^{15}$ s^{-1} and collision frequency $\gamma_m=12.18\times10^{13}$ s^{-1}), and $\varepsilon^{(0)}=1$. Using the Drude dispersion model one takes automatically into account the mass and any kinetic energy of the current-carrying electrons inside the metal (the contribution of the bound electrons is also taken into account through the constant $\varepsilon^{(0)}$).

The calculations presented here have been performed using the finite integration technique, employed through the MICROWAVE STUDIO (MWS) commercial software package. Using MWS, the transmission and reflection from a monolayer of the structure have been obtained; these data have been used for the determination of the effective permittivity and permeability of the structures through a standard retrieval procedure based on a homogeneous effective-medium approach.[44,45] This way we obtain the effective permeability, μ, and permittivity, ϵ, valid for bulk metamaterials of many unit cells (layers) along the propagation direction[46] (rather than μ and ϵ characterizing a single sheet of scatterers[47]). Although the use of the homogeneous effective-medium approach for such kinds of metamaterials has been proven not to be fully adequate[48–50] (since the influence of periodicity and spatial dispersion effects are quite substantial), we have observed here that for normal incidence and specific wave polarization we still can define and use such effective parameters, except in the frequency regimes very close to the resonance frequencies (where the wavelength inside the structure, $\lambda_{in}=\lambda_0/n_e$, is comparable to the structure linear size; λ_0 is the free-space wavelength and n_e the real part of the effective refractive index). Values of effective parameters in frequency regimes very close to resonances will not been used throughout this paper. Note also that frequency regimes very close to μ resonance are regimes of very high losses [since the Im(μ) gets its highest values there] and thus they are not of interest for the achievement of left-handed materials.

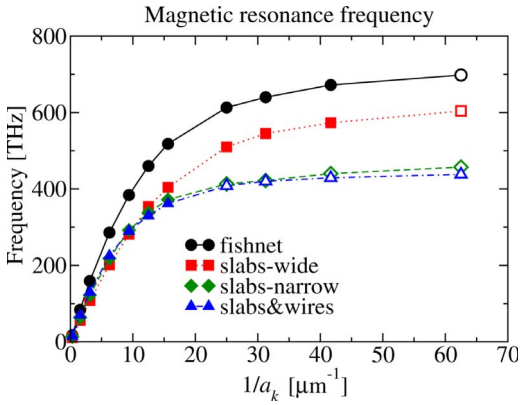

FIG. 2. (Color online) Scaling of the magnetic-resonance frequency with the linear size of the unit cell along propagation direction (a_k) for the four designs of Fig. 1: fishnet (black circles), wide slabs (red squares), narrow slabs (green diamonds), and slabs&wires (blue triangles). The solid symbols indicate the existence of negative permittivity values while the open symbols indicate that the permeability resonance is weak and unable to reach negative values for the Re(μ).

In Fig. 2 we present the magnetic-resonance frequency for the four structures of Fig. 1 as the structures are scaled down from millimeter to nanometer scale; in Fig. 3 we show the real and imaginary parts of the magnetic permeability as a function of frequency, for wide-slab pairs [the structure in Fig. 1(b)] of various length scales.

As can be seen in Fig. 2, in slab-pair systems we observe the same behavior as the one reported earlier for SRR structures:[37,42] while for larger length scales the magnetic-resonance frequency scales inversely proportional to the structure linear size, at frequencies in the near IR toward optical regime this linear scaling breaks down, and the magnetic-resonance frequency saturates to a constant value. This saturation value is different for the different designs employed, with the larger one being that of the fishnet structure. Note that in the slabs&wires case [structure in Fig. 1(c)] the presence of wires does not affect the magnetic-resonance frequency of the slabs while in the fishnet structure the presence of wires leads to a higher saturation value for the magnetic-resonance frequency. This behavior of the fishnet design will be discussed and explained in Sec. IV.

It is important to mention here that the saturation values for the magnetic-resonance frequency of the slab-pair systems are in all cases larger than the saturation values obtained for SRRs of a single gap[51] (e.g., U-shaped SRRs; single-gap SRRs are the only SRR-based system that has been fabricated in the nanometer scale), indicating once more the suitability of the slab-pair-based systems for the achievement of optical magnetic metamaterials.

Concerning the permeability results shown in Fig. 3, we observe that, similarly to the SRRs,[37,42] as the length scale of the structure becomes smaller the permeability resonance becomes weaker, ceasing ultimately to reach negative values. This weakening is revealed in both the real and imaginary

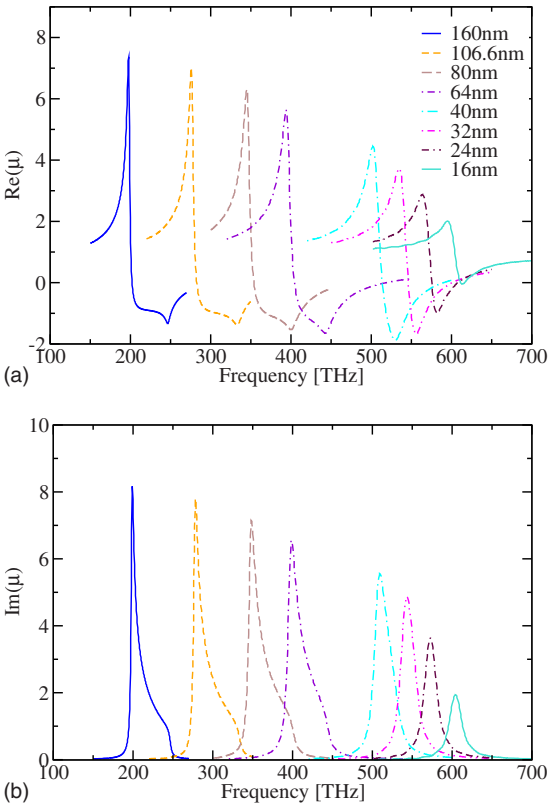

FIG. 3. (Color online) Frequency dependence of the real (top panel) and the imaginary (bottom panel) part of the magnetic permeability of the wide-slab-pair system for various length scales. The legends indicate the lattice constant along propagation direction for each specific system.

parts of the permeability resonance, and it will be analyzed in more detail and quantified in the following paragraphs. (Note that the "truncation" of the resonances of Fig. 3, which is observed in the larger scale structures, is an artifact coming from the limited validity of the homogeneous effective-medium approach in the frequency regimes close to the resonances, due to periodicity influence and spatial dispersion effects, as was mentioned earlier in this section. For smaller scales this influence becomes smaller due to the deeper subwavelength scale of the corresponding structures and the weaker resonant response, which results in a smaller effective index and thus a larger wavelength inside the structures.)

One quantity which is of great interest in left-handed materials and is strongly affected by the weakening of the permeability resonance is the width of the negative permeability regime, which roughly corresponds to the operational bandwidth of a LHM. In Fig. 4 we present the relative bandwidth (i.e., bandwidth divided by the lower frequency of the negative permeability band) for the four structures shown in Fig. 1. As can be seen in Fig. 4, the operational bandwidth, which for larger scales is almost independent of the length scale, in smaller scales is strongly reduced, ultimately going to zero for all designs. This shows that the negative permeability is ultimately killed in the nanometer scale structures. Among our four structures the wide-slab-pair one is characterized by the larger bandwidth. Finally, it is worth noticing the highly reduced bandwidth of the fishnet design, compared to the

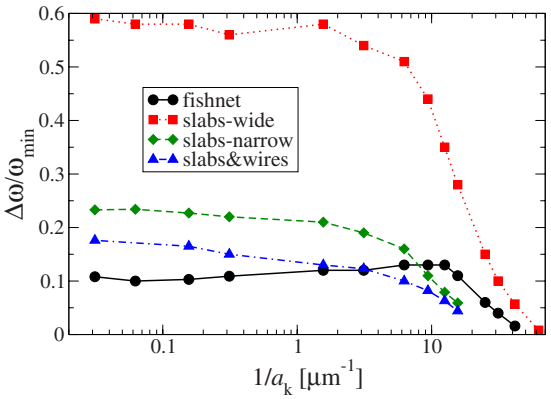

FIG. 4. (Color online) Bandwidth, $\Delta\omega$, of the negative magnetic permeability regime vs the inverse unit-cell size, $1/a_{\mathbf{k}}$, for fishnet (black circles), wide-slab pairs (red squares), narrow-slab pairs (green diamonds), and slabs&wires (blue triangles). The bandwidth is normalized by the minimum frequency (lower limit) of the negative permeability regime, $\omega_{\min}$. $a_{\mathbf{k}}$ is the lattice constant along propagation direction.

bandwidth of the slab-pair-only structure. This bandwidth behavior will be discussed in the next section.

Since one of the main issues for the achievement of high-frequency metamaterials of satisfactory performance is the losses (due to the increased resistive losses in the metallic components going to the optical regime), we performed a detailed analysis of the losses in high-frequency metamaterials, trying to estimate which aspects of the high-frequency metamaterial response are mainly affected by the resistive losses and, consequently, to seek ways to minimize the influence of those losses, using proper design modifications.

As a first step we calculate the losses as a function of frequency for various length scales of our systems. In Fig. 5 we present these losses for the wide-slab-pair system of Fig. 1(b). The losses, A, have been calculated through the relation $A=1-R-T$, where R and T are the reflection and transmission coefficients, respectively, through one unit cell of the structure along the propagation direction. As is expected, the losses show a dramatic increase by going to smaller length

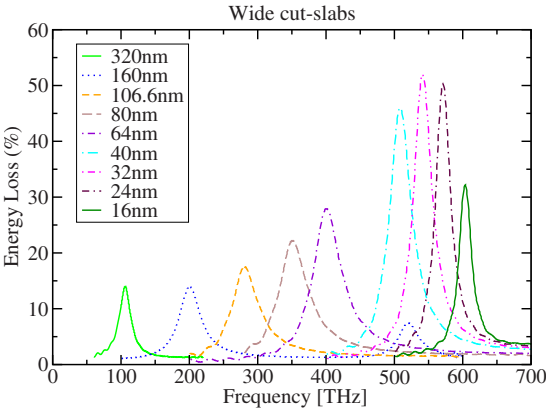

FIG. 5. (Color online) Loss, A, per unit cell (%) for the wide-slab-pair system for various length scales of the system, close to the magnetic-resonance frequency saturation regime. The legends indicate the lattice constant along propagation direction.

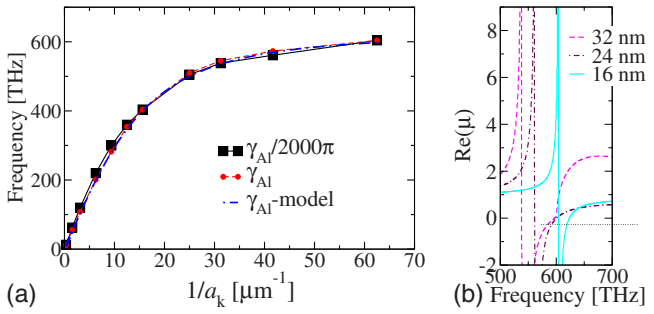

FIG. 6. (Color online) (a) Saturation of the magnetic-resonance frequency for the wide-slab-pair structure using for the metal a 2000π times reduced collision frequency compared with that of aluminum, i.e., $\gamma_m=\gamma_{Al}/2000\pi$ (solid-black line with squares). For comparison the corresponding result for $\gamma_m=\gamma_{Al}$ is given (dashed-red line with circles). Dotted-dashed line (blue color) shows the scaling of the magnetic-resonance frequency as it is obtained from our RLC circuit model (for the γ_{Al} case). (b) Magnetic permeability resonance [shown in Re(μ)] as a function of frequency for the wide-slab-pair structure of Fig. 1(b), for $\gamma_m=\gamma_{Al}/2000\pi$ and for three different structure length scales. Legends denote the lattice constant along propagation direction, $a_{\mathbf{k}}$.

scales and higher frequencies. This increase seems to have an exponential dependence on the magnetic-resonance frequency.

From Figs. 2–5, one can see clearly the decreased performance of our structures going to nanometer scales, inhibiting their ability to give high quality optical left-handed metamaterials. An interesting question arising here is *the role of the resistive losses* on this decreased performance. To examine this role, we repeated the above calculations using for the metal a $2\pi\times1000$ times reduced collision frequency compared to that of aluminum, i.e., $\gamma_m=12.18\times10^{10}/2\pi$. The results concerning the wide-slab-pair system are shown in Fig. 6.

Specifically, Fig. 6(a) shows the saturation of the magnetic-resonance frequency and Fig. 6(b) the real part of the resonant permeability response for the smaller length scales. Comparing the result of Fig. 6 with those for the nonreduced value of γ_m, one can see that the saturation of the magnetic-resonance frequency seems to be totally unaffected by the value of the metal collision frequency. This indicates that the loss factor of the metal employed is not able to affect the highest achievable magnetic-resonance frequency of each specific design. On the other hand, the metal loss factor can affect the minimum length scale able to give a negative permeability response, as shown by comparing Fig. 6(b) with Fig. 3(a). Indeed, in the small γ_m cases the magnetic permeability resonance is quite stronger, maintaining negative values down to smaller length scales. Although the strength of the resonance [as measured, e.g., by the minimum value of the Re(μ)] seems to be strongly affected by the γ_m value, calculating the width of the negative permeability regime (in the cases that such a regime exists), $\Delta\omega$—not shown here—it is observed that it is only slightly affected by the γ_m value; it tends to zero for both high and low values of γ_m, indicating that even in the absence of resistive losses one cannot go to an arbitrarily high-frequency negative permeability response over a practical bandwidth.

The results presented above raise many questions concerning the high-frequency magnetic metamaterial response and the main phenomena and factors determining this response. Before attempting an interpretation of this response we will summarize here the main effects observed so far and the main questions that one needs to address so as to clarify and to be able to predict the existence or performance of an optical negative magnetic permeability response.

(a) The magnetic-resonance frequency of slab-pair-based systems, while in millimeter scale structures, scales inversely proportional to the structure length scale, in submicrometer scale structures saturates to a constant value, depending mainly on the geometry of the structure and independent of the resistive losses in the component materials. Among the structures that have been studied here the fishnet design leads to the highest saturation frequency. Moreover, while in the slabs&wires design the magnetic-resonance frequency is almost unaffected by the presence of the wires, it is not the same in the fishnet design, where the saturation value is much higher than the saturation value for the slabs only case.

(b) The magnetic permeability resonance in submicrometer scale structures becomes more and more weak by reducing the structure length scale, and ultimately ceases to reach negative values. The length scale at which $\mu<0$ stops to exist depends on the structure geometry (design) and on the resistive losses in the component materials, especially in the metallic parts. Among the structures that we have examined, negative permeability in smaller length scales is achieved in the slab-pair structures, not associated though with higher magnetic-resonance frequency. Negative permeability at higher frequencies is achieved in the fishnet design.

(c) Concerning the relative spectral width of the negative permeability regime, this width, while it is constant in millimeter scale structures, as one goes toward nanometer scales it becomes smaller and smaller, down to almost vanishing. This width depends on the structure geometry and seems only slightly dependent on the resistive metallic losses.

III. ANALYTICAL MODEL AND INTERPRETATION OF THE RESULTS

To understand and explain the results presented in the previous section, we use the common approach of describing the artificial magnetic structures (at the resonant magnetic response regime) as equivalent effective RLC circuits (see Fig. 7). Using circuit theory and basic electromagnetic considerations,[3] one can easily obtain an expression for the frequency dependence of the effective magnetic permeability, $\mu(\omega)$, for a lattice of artificial magnetic elements.[3]

For the explanation of the high-frequency magnetic response we follow the approach of Ref. 37, based on the consideration of the kinetic energy of the electrons in the metal, E_k, besides the magnetic energy of the resulting electromagnetic field. Thus, we replace the magnetic inductance of the system in the effective RLC circuit description by the total inductance resulting as a sum of the magnetic field inductance, L, and the kinetic inductance, L_e, where L_e is defined by $E_k=N_e m_e v_e^2/2=L_e I^2/2$ (N_e is the total number of electrons, m_e is the electron mass, and v_e is the average electron velocity).

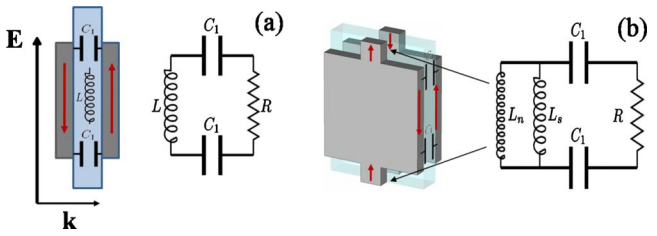

FIG. 7. (Color online) The equivalent RLC circuit used for the description of our slab-pair systems [panel (a)] and for the fishnet design [panel (b)]. Figure 7 also shows the correspondence of the RLC circuit parameters with our structures. The arrows show the direction of the currents at the magnetic-resonance frequency. The total capacitance of the circuits, C, is equal to $C_1/2$. For the fishnet design $L_s=L_{\text{slabs}}$ is the slab contribution to the inductance and $L_n=L_{\text{necks}}$ is the contribution from the neck parts.

Assuming a slab-pair system like the one shown in Fig. 1(e), of length l and slab separation t, excited by a magnetic field of the form $H=H_0e^{-i\omega t}$ and direction as shown in Fig. 1(e), and applying the Kirchhoff voltage rule, one can obtain

$$(L+L_e)\ddot{I}+\frac{1}{C}I+\dot{I}R=-\ddot{\phi}=\omega^2\mu_0 ltH_0e^{-i\omega t}. \tag{1}$$

ϕ is the external magnetic flux, $\phi=\mu_0 ltH$, and R and C the resistance (frequency independent, accounting for the ohmic losses) and the capacitance of the system, respectively. The obvious solution of Eq. (1) is $I=I_0e^{-i\omega t}$, with

$$I_0=-\frac{\omega^2[\mu_0 lt/(L+L_e)]}{\omega^2-1/(L+L_e)C+i\omega R/(L+L_e)}H_0. \tag{2}$$

Having the current one can easily obtain the pair magnetic dipole moment, $m=\text{area}\times\text{current}=ltI$, and the magnetization $M=(N_{LC}/V)ltI=(1/V_{uc})ltI$, N_{LC} is the number of "RLC" circuits in the volume V, and $V_{uc}=a_{\mathbf{E}}a_{\mathbf{H}}a_{\mathbf{k}}$ is the volume per unit cell, where $a_{\mathbf{E}}$, $a_{\mathbf{H}}$, and $a_{\mathbf{k}}$ are the system lattice constants along the **E**, **H**, and **k** directions, respectively ($a_{\mathbf{H}}\geq w, a_{\mathbf{E}}>l, a_{\mathbf{k}}\geq t$)—see Fig. 1).

Finally, using $M=\chi_m(\omega)H$, $\mu(\omega)/\mu_0=1+\chi_m(\omega)$, with χ_m the magnetic susceptibility, one obtains

$$\mu(\omega)=\mu_0\left\{1-\frac{(1/V_{uc})[\mu_0(lt)^2/(L+L_e)]\omega^2}{\omega^2-\omega_{LC}^2+i\omega\gamma}\right\} \tag{3}$$

with

$$\omega_{LC}=\frac{1}{\sqrt{(L+L_e)C}},\quad \gamma=\frac{R}{L+L_e}. \tag{4}$$

ω_{LC} is the magnetic-resonance frequency of the system and γ is the dumping factor, representing all the losses and the scattering mechanisms.

The inductance L_e can be easily calculated by calculating the kinetic energy of the electrons, $E_k=N_em_ev_e^2/2=2V_wn_em_ev_e^2/2$, and expressing the velocity through the current, $I=ewt_mn_ev_e$ [n_e is the number density of free electrons, e is the electron charge, and $V_w=wt_ml$ is the volume of each metallic slab of the pair—see Fig. 1(e)]. In this way, one can obtain $L_e=2lm_e/wt_me^2n_e=(2l/wt_m)(1/\omega_p^2\varepsilon_0)$, where $\omega_p=\sqrt{e^2n_e/m_e\varepsilon_0}$ is the plasma frequency of the bulk metal.

Note that exactly the same results as in Eq. (3) can be obtained by considering, instead of the kinetic energy for the derivation of L_e, the dispersive behavior of the metal conductivity. Indeed, starting with the frequency-dependent Drude-type conductivity

$$\sigma=i\varepsilon_0\frac{\omega_p^2}{\omega+i\gamma_m}, \tag{5}$$

we obtain for the total resistance (for both slabs of the pair)

$$R_{tot}=\frac{1}{\sigma}\frac{2l}{S}=\left(\frac{\gamma_m}{\varepsilon_0\omega_p^2}-i\frac{\omega}{\varepsilon_0\omega_p^2}\right)\frac{2l}{S}=R-i\omega L_e. \tag{6}$$

Using $R_{tot}=R-i\omega L_e$ in Eq. (1) in the place of R and only the magnetic field inductance (in order to avoid counting twice the kinetic inductance L_e), one can obtain the same current solution as in Eq. (2).

In the following, to simplify our discussion we will consider the magnetic field inductance to be given by the inductance of a solenoid of area lt and length w (see Fig. 1), i.e., $L=\mu_0 lt/w$, and the total capacitance, C, by that of two parallel-plate capacitors connected in series (see Fig. 7), each one of area wl_C, plate separation t and dielectric core of relative dielectric constant ε_b, i.e., $C=C_1/2=\varepsilon_0\varepsilon_b(wl_C)/2t$. C_1 is the capacitance of each capacitor and l_C the effective length of the capacitor, proportional to the slab length, l, i.e., $l_C=c_1l$, with the constant c_1 approximately equal to 0.4 (see Sec. V), as is revealed from the charge distribution at the magnetic resonance. [Note that these formulas are appropriate for the case of wide slabs; for the case of narrow slabs, where edge effects become important, the capacitance and the inductance get slightly higher values (the scaling dependence though remains the same); such more accurate values can be reproduced by more complicated formulas for the capacitance and inductance. Here, since we are interested mainly in general trends and in providing a simple and uniform for all our structures physical picture and qualitative explanation, we will not be extending to more complicated inductance and capacitance formulas. Note also that in our discussion we will not consider any interunit-cell capacitance,[26] which is important in the case of quite long slabs, i.e., slabs that approach the unit-cell boundaries along **E** direction.]

With the above considerations, Eq. (3) for the magnetic permeability takes the form

$$\mu=\mu_0\left[1-\frac{F'\omega^2}{\omega^2-\omega_{LC}^2+i\omega\gamma}\right] \tag{7}$$

with

$$F'=F\frac{L}{L+L_e},\quad F=\frac{ltw}{V_{uc}}=\frac{\text{interpair volume}}{\text{unit-cell volume}}. \tag{8}$$

Using the above formulas and their behavior going to small length scales we will show in the following that one can reproduce and explain all the high-frequency magnetic response of artificial magnetic structures.

For that, it is important to notice that by scaling down the structures uniformly, i.e., all the lengths scale proportionally to a basic length a ($=a_{\mathbf{k}}$ here), both the capacitance and the magnetic inductance scale proportionally to a (this scaling law is valid not only for our simple formulas but for all possible capacitance and inductance formulas) while the kinetic inductance and the resistance scale proportionally to $1/a$, i.e.,

$$C = \frac{c_1}{2}\varepsilon_0\varepsilon_b\frac{wl}{t} \sim a, \quad L = \mu_0\frac{tl}{w} \sim a,$$

$$R = \frac{\gamma_m}{\omega_p^2\varepsilon_0}\frac{2l}{wt_m} \sim \frac{1}{a}, \quad \text{and} \quad L_e = \frac{2l}{wt_m}\frac{1}{\omega_p^2\varepsilon_0} \sim \frac{1}{a}. \tag{9}$$

The above formulas show the increasingly pronounced role that kinetic inductance (also the resistance) plays in the smaller scales. Specifically, one can see that the ratio L/L_e is on the order of $20tt_m/\lambda_p^2$, with the typical value of $\lambda_p(\lambda_p = 2\pi c/\omega_p)$ being around 85 nm for Al and 130 for Ag.[52] Thus, for $\sqrt{tt_m}$ smaller than 100 nm the kinetic inductance, L_e, becomes appreciable and may dominate as the length scale becomes smaller and smaller.

A. Magnetic-resonance frequency

Taking into account the expression for the magnetic-resonance frequency in Eq. (4), in combination with Eq. (9), it can be shown that the magnetic-resonance frequency of a slab-pair system has the following scale dependence:

$$\omega_{LC} = \frac{1}{\sqrt{(L+L_e)C}} \propto \frac{1}{\sqrt{A_1a^2 + A_2}} \tag{10}$$

with the A_1 and A_2 constants (depending on the geometrical characteristics of the structure). Equation (10) shows that as the slabs length scale becomes smaller the magnetic-resonance frequency does not continuously increase but beyond a length scale it saturates to a constant value. The saturation of the magnetic-resonance frequency is exactly what is observed in Fig. 2 and is exclusively due to the existence of kinetic inductance [note that the resistance, R, representing the ohmic losses, does not appear in the above formula (10)]. This inductance originates from the electron inertia and represents the "difficulty" of electrons to follow high-frequency motions, i.e., their difficulty to respond to high-frequency fields.

Note that without the consideration of L_e the second term in the square root of Eq. (10) would not exist, leading to a linear dependence $\omega \sim 1/a$ (as occurs in microwaves and larger scales) making us unable to explain the saturation behavior observed in Fig. 2. Note also that the kinetic inductance L_e does not influence the response of the structure only at the magnetic-resonance regime but at all high-frequency regimes, including permittivity resonances.

Substituting Eq. (9) in Eq. (10) and defining normalized (dimensionless) geometrical parameters, i.e., $l'=l/a$, $t'=t/a$, and $t'_m=t_m/a$, one can obtain the dependence of ω_{LC} from the geometrical characteristics of the structure, as well as an expression for the saturation value, ω_{LC}^{sat},

$$\omega_{LC} = \frac{1}{\sqrt{\frac{c_1}{2}\frac{\varepsilon_b l'^2}{c^2}a^2 + \frac{c_1\varepsilon_b l'^2}{t't'_m\omega_p^2}}} \underset{a\to 0}{\to} \omega_p\frac{\sqrt{t't'_m}}{l'\sqrt{c_1\varepsilon_b}} = \omega_{LC}^{\text{sat}}. \tag{11}$$

A correction to the above formula (11) can be obtained if one takes into account also the potential energy of the electrons inside the metal slabs through an equivalent capacitance,[38] $C_e=\varepsilon_0 wt_m/l$ (the capacitance of the capacitor formed inside the metal), added to the slabs capacitance, C_1. In this case the saturation value for the magnetic-resonance frequency is found as

$$\omega_{LC}^{\text{sat}} = \frac{\omega_p}{\sqrt{\frac{c_1\varepsilon_b l'^2}{t't'_m} + 1}}, \tag{12}$$

showing that the absolute upper limit for the saturation frequency is not arbitrary high but it is restricted by the plasma frequency of the bulk metal.

Since in the following we will consider systems with both l'/t' and l'/t'_m larger than unity, where the simplified Eq. (11) is still valid, we will omit the electron potential energy in the following discussion, keeping into account though that this energy/capacitance sets a finite upper limit for the saturation value of the magnetic-resonance frequency, which is the plasma frequency of the bulk metal.

B. Magnetic permeability resonance

As has been shown in Sec. II, by reducing the length scale of the artificial magnetic structures the magnetic permeability resonance becomes more and more weak, and unable to lead to negative μ values beyond a certain length scale. This weakening is revealed in both the real part of μ (where smaller absolute values of the Max[Re(μ)] and Min[Re(μ)] are observed) and the imaginary part (where smaller Max[Im(μ)], at $\omega=\omega_{LC}$, is observed)—see Fig. 3.

A detailed examination of Eq. (7) reveals that the strength of the resonance is determined from both factors γ and F'. On the other hand, the width of the negative permeability regime, $\Delta\omega$, seems to be much more sensitive to the factor F' and almost unaffected by γ (γ has only small influence on the lower limit of the negative permeability band while F' strongly affects the upper limit of this band). Note that in the absence of losses, i.e., $\gamma=0$, the upper limit of the negative permeability band is $\omega_{LC}/\sqrt{1-F'}$; the lower limit is simply ω_{LC}, i.e.,

$$\Delta\omega = \omega_{LC}\left(\frac{1}{\sqrt{1-F'}} - 1\right). \tag{13}$$

Using Eqs. (4) and (8) in combination with Eq. (9), one can obtain the scaling dependence of both F' and γ, as

$$F' = F\frac{L}{L+L_e} \propto BFa^2 \tag{14}$$

(B constant) and

$$\gamma = \frac{R}{L + L_e} \propto \frac{1}{D_1 a^2 + D_2} \tag{15}$$

(D_1 and D_2 constants). From Eq. (14) one can derive two important conclusions: (a) the factor F', which mainly determines the frequency width of the negative permeability regime, is independent of the resistance, R, thus independent of any loss mechanisms. (b) With the consideration of the kinetic inductance the factor F' from scale independent (if L_e is negligible) becomes scale dependent and tends to zero as the size of the structure becomes smaller and smaller ($a \rightarrow 0$). This means that even in the absence of ohmic losses, it would be impossible to get negative permeability values of bandwidth substantially larger than $(a^2/\lambda_p^2)\omega_{LC}$ for arbitrarily small length scales.

The scaling behavior of F' also implies that the relative bandwidth of the negative permeability regime while it is almost constant before the starting of the saturation (see Fig. 4), it becomes smaller and smaller deeper in the saturation regime, indicating that working before the saturation regime favors the widest bandwidth of each specific structure.

The geometrical dependence of the factor F' for the slab-pair design can be easily obtained by substituting Eq. (9) to Eq. (14):

$$F' = F\frac{1}{1 + 2c^2/(\omega_p^2 t_m t)} = \frac{F}{1 + \lambda_p^2/(2\pi^2 t t_m)}. \tag{16}$$

Concerning the loss factor γ, from Eq. (15) one can see that γ increases as the length scale decreases, justifying the higher losses for the smaller length scales. This increase though does not continue up to the smallest scales but beyond a certain length scale it approaches a saturation value. The geometrical dependence of γ for the slab-pair design is obtained analogously with that of F', as

$$\gamma = \frac{\gamma_m}{1 + (\omega_p^2/2c^2) t_m t} = \frac{\gamma_m}{1 + 2\pi^2 t_m t/\lambda_p^2}. \tag{17}$$

Equation (17) shows that the saturation value of γ is the collision frequency of the bulk metal as considered in the free-electron (Drude) description of the metal.[53] The saturation regime for γ is approached simultaneously with that of the magnetic-resonance frequency saturation, showing that deep in the saturation regime the weakening of the resonance is not mainly the result of the ohmic losses but it is rather the result of the kinetic inductance (affecting through the factor F').

Finally, it is important to point out that both γ and F' depend not only on the "quality" (i.e., plasma frequency and damping factor) of the metal used for the fabrication of metamaterials but also on the geometrical parameters of the structures [see Eqs. (16) and (17)]. This reveals the possibility to modify these factors, and thus to enhance the performance of high-frequency metamaterials, by modifying the geometry.

IV. OPTIMIZED DESIGNS

From the analytical formulas and the discussion of the previous section it becomes clear that for achievement of optimized high-frequency (e.g., optical) magnetic metamaterials one should require: (a) highest possible saturation value for the magnetic-resonance frequency; (b) larger possible parameter F', determining the strength of the magnetic resonance and the width of the negative permeability regime; and (c) smallest possible loss factor γ.

The general requirements for meeting the above conditions can be easily concluded based on Eqs. (10), (14), and (15). They demand: structures of small capacitance, C; structures of small kinetic inductance L_e, compared with magnetic inductance, L; and structures of low resistance, R. On the other hand, the role of the magnetic field inductance is more puzzling: while low inductance facilitates the achievement of high magnetic-resonance frequency, it results in a "lower-quality" resonance, i.e., weaker resonance and higher losses (compared to a higher inductance structure of the same length scale). Thus, the inductance optimization should be based on the specific requirements for the designed metamaterial.

To translate the above optimization conditions to specific geometrical and material conditions for the slab-pair-based systems we can use Eqs. (11), (16), and (17). From these equations it can be concluded that optimized slab-pair-based systems are favored from structures of thick metal (high t_m) and thick separation layer between the slabs of the pair (i.e., high t—not as high though as to cancel the interaction between the slabs); also structures of wide slabs [i.e., large width w—to maximize the structure volume fraction F appearing in Eq. (16)]. Moreover, high quality optical metamaterials demand metals of the highest possible plasma frequency and the lowest possible collision frequency.

The role of the slab length is not one way; while shorter slabs (compared to the corresponding unit-cell side) facilitate a high magnetic-resonance frequency they lead to a narrower negative permeability regime [due to reduced F in Eq. (16)] and vice versa. Finally, we should emphasize here that for enhanced metamaterial performance one should target operation below the saturation regime, so as to ensure a large negative permeability width and lower losses.

Fishnet design

As was mentioned in the previous sections and can be easily concluded from Eq. (10), structures with reduced inductance lead to higher magnetic-resonance frequencies. A structure based on slab pairs which offers a considerable reduction in the inductance is the fishnet design—see Fig. 1(d). Studies of this design in microwaves[29] have revealed that at the magnetic-resonance loop currents exist not only at the slab pair but also in the necks' part of the metallic element. This neck contribution can be taken into account in an effective LC circuit description of the structure by considering an additional inductance, due to the necks, which is in parallel with the inductance of the slabs [see Fig. 7(b)], resulting in a reduced total inductance, L_{fishnet}, with

$$\frac{1}{L_{\text{fishnet}}} = \frac{1}{L_{\text{slabs}}} + \frac{1}{L_{\text{necks}}}. \tag{18}$$

(L_{slabs} and L_{necks} represent the inductance of the slab and the neck parts, respectively; note that the L_{slabs} here is not ex-

actly the same as that for the slab-pair-only system, due to the difference in the charge and current distribution between only-slab-pair systems and fishnet.) This reduced inductance leads to a magnetic-resonance frequency

$$\omega_{LC,\text{fishnet}}^2 = \frac{1}{L_{\text{fishnet}}C} \approx \omega_{LC,\text{slabs}}^2\left(1+\frac{L_{\text{slabs}}}{L_{\text{necks}}}\right), \qquad (19)$$

i.e., higher than that of only the slabs.

By reducing the size of the structure down to submicron and nanometer scales, the inductance of both the slab and the neck parts gets a contribution from the kinetic (electrons) inductance. This contribution though does not modify the general relation (19), indicating the higher magnetic-resonance frequency of the fishnet design than that of the component wide-slab-pair system even in the saturation regime. This higher magnetic-resonance frequency makes the fishnet design the preferred one for the achievement of optical metamaterials, something that has already been revealed from many previous experimental and theoretical works concerning optical metamaterials.[18,19]

Relation (19), combined with Eq. (9), can easily lead to a relation for the geometrical dependence of the magnetic-resonance frequency for the fishnet, i.e.,

$$\omega_{LC,\text{fishnet}}^2 = \omega_{LC,\text{slabs}}^2\left(1+\frac{w_n}{w}\frac{l}{a_{\mathbf{E}}-l}\right) \qquad (20)$$

and thus for the saturation value of this magnetic-resonance frequency. In Eq. (20) w_n and w is the width of the neck and slab parts, respectively (along **H** direction) and $a_{\mathbf{E}}$ is the lattice constant along the **E** direction (see Fig. 1). Equation (20) suggests that for the achievement of high magnetic-resonance frequency saturation values for fishnet, apart from the conditions for the optimization of the slab-pair components one should pursue also wide neck parts; moreover, the wider the neck parts the higher the saturation value of the fishnet magnetic-resonance frequency is.

Concerning the magnetic permeability expression for the fishnet, here the situation is more complicated compared to only-slab systems due to the more complicated current picture at the magnetic resonance.[29] Following the observations and conclusions of Ref. 29, according to which the fishnet unit cell can be approximated with an RLC circuit with inductance of slabs and inductance of necks connected in parallel, the magnetic permeability for the fishnet can be calculated following the same steps as the ones presented in the previous section for the slab case, with modifications in the incident flux, the magnetic moment, and the total inductance per unit cell:

Here the incident flux, ϕ, can be written as $\phi = \mu_0 a_{\mathbf{E}} t H_0 e^{-i\omega t}$, and the modified magnetic moment as

$$m = I_{\text{slabs}} l t - I_{\text{necks}}(a_E - l)t = I L_{\text{fishnet}}\left[\frac{lt}{L_{\text{slabs}}} - \frac{(a_{\mathbf{E}}-l)t}{L_{\text{necks}}}\right], \qquad (21)$$

where $I = I_{\text{slabs}} + I_{\text{necks}}$ and $I L_{\text{fishnet}} = I_{\text{slabs}} L_{\text{slabs}} = I_{\text{necks}} L_{\text{necks}}$.

The inductances L_{slabs} and L_{necks} include both the magnetic field inductance and the electrons inductance for slabs and necks.

From Eq. (21) one can see already that the presence of the necks weakens the magnetic response of the structure since the neck contribution in the magnetic moment opposes that of the slabs.

With the above considerations, the magnetic permeability for the fishnet design can be expressed as

$$\mu(\omega) = \mu_0\left\{1 - \frac{(1/V_{uc})\mu_0 a_E t \omega^2 [lt/L_{\text{slabs}} - (a_E - l)t/L_{\text{necks}}]}{\omega^2 - 1/L_{\text{fishnet}}C + i\omega R/L_{\text{fishnet}}}\right\}. \qquad (22)$$

Comparing the above equation with Eq. (3), one can observe that the factor multiplying the ω^2 in the numerator, which is the main factor determining the spectral width of the negative permeability regime, becomes smaller than that of the slab only case (F'). This can explain the reduced (compared to only slabs) spectral width of the fishnet negative μ regime observed in Fig. 4.

V. OBTAINING QUANTITATIVE RESULTS

In the previous sections we presented a simple RLC circuit model for our slab-pair-based metamaterial structures. This model allows for a simple physical and uniform description of all our structures, resulting in a simple physical interpretation for the behavior of the structures, reproducing the main features of their response, and leading to easy to understand optimization rules. It is important to note though that relations (3) and (4) do not only have a qualitative power but they can be used also to obtain quantitative results, if plugged with accurate expressions for the capacitances and inductances involved.

Here we will demonstrate this quantitative power of relations (3) and (4) in the case of the wide-slab-pair system. For wide-slab-pair systems ($w = a_{\mathbf{H}}$) and examining the fields and currents at the magnetic-resonance frequency, one can use for the capacitance C_1 (see Fig. 7) the formula shown in Eq. (9) with $c_1 = 0.4$, i.e., $C_1 = \epsilon_0\epsilon_b(w/t)(0.4l)$, and for the magnetic field inductance and electrons' inductance the same relations as in Eq. (9). The calculated magnetic-resonance frequency obtained this way is shown with the dotted-dashed line in Fig. 6 and as can be seen there it is in excellent agreement with the magnetic-resonance frequency obtained through realistic numerical simulations.

Using the same equations for L and C for the case of narrow slabs, one can observe that the quantitative agreement with the corresponding numerical data is less satisfactory; the reason is the increased importance of edge effects as the slabs become narrower, which would lead to an enhancement of L and C. Ways to take into account these effects are either using an artificial, higher value of c_1 in the capacitance C_1 or employing more complicated formulas for the capacitance and inductance of the structure. In the limit $w < t$ such formulas can be the formulas describing a system of two parallel wires, i.e., $L = \mu_0 l \ln(t/w)/\pi$ and $C_1 = \epsilon_b\epsilon_0\pi(l_C)/\ln(t/w)$. Note that the employment of alternative expressions for L and C_1 does not change the general features of the scaling response of the structure.

As a last statement we should mention here that to proceed to a detailed quantitative description of our structures,

able to reproduce experimental data, besides the requirement of accurate formulas for the capacitance and the inductance, one should also employ an accurate dispersion model for the metal dielectric function (note that for the majority of the metals the Drude dispersion model is not valid in the whole IR and visible regime[52]—due mainly to interband transitions) and take into account that in the IR the skin depth of the metal is smaller than the metal thickness.

VI. CONCLUSIONS

In this paper we examine the magnetic response of resonant magnetic structures based on the slab-pair design, as the structures are scaled down from millimeter to nanometer scale. This response is examined using detailed numerical simulations to obtain the frequency dependence of the magnetic permeability (including its resonant behavior) through reflection and transmission data of realistic structures. It is observed, as expected, that the magnetic-resonance frequency of the structures while it scales inversely proportional to the structure length scale in the millimeter scale, it saturates to a constant value in the nanoregime. This behavior depends on the design and it is independent of any ohmic losses in the structure. Among our designs, a higher saturation value is observed for the fishnet design.

The permeability resonance becomes weaker and weaker as we go deeper into the submicrometer scale and ultimately it does not reach negative values. The relative spectral width of the negative permeability regime which in larger scales is almost scale independent, in submicrometer scales it becomes smaller and smaller, approaching zero, and it has a very slight dependence on the ohmic losses while it shows a strong dependence on the design, being quite narrow for the fishnet design.

All the above results are explained through a simple RLC circuit model; in the inductance, L, the current-connected kinetic energy of the electrons is also taken into account besides the magnetic field energy. This model had the capability to determine the optimization conditions for our structures, so as to attain high magnetic-resonance frequencies, maintaining strong resonant response with a negative permeability region as wide as possible. The model explains also the superior performance of the fishnet design regarding high magnetic-resonance frequency and its reduced performance regarding the width of the negative permeability region. Finally, we show that our simple RLC circuit model is capable not only of predicting qualitatively the behavior of our structures but also to give quantitative results if it is accompanied by accurate formulas for the capacitance and inductance of the systems.

ACKNOWLEDGMENTS

Authors would like to acknowledge financial support by the European Union FP7 projects PHOME, ENSEMBLE, ECONAM, NIMNIL, and the COST Actions MP0702 and MP0803, by the European Office of Aerospace Research and Development (under project FENIM), and by the U.S. Department of Energy (Contract No. DE-AC02-07-CH11358).

*kafesaki@iesl.forth.gr

[1] V. G. Veselago, Sov. Phys. Usp. **10**, 509 (1968).
[2] For reviews see J. B. Pendry, Contemp. Phys. **45**, 191 (2004); J. B. Pendry and D. R. Smith, Phys. Today **57**(6), 37 (2004).
[3] C. M. Soukoulis, M. Kafesaki, and E. N. Economou, Adv. Mater. **18**, 1941 (2006).
[4] *Handbook of Artificial Materials*, edited by F. Capolino (CRC Press, Cleveland, 2009), Vol. 1.
[5] J. B. Pendry, Phys. Rev. Lett. **85**, 3966 (2000).
[6] D. R. Smith, Willie J. Padilla, D. C. Vier, S. C. Nemat-Nasser, and S. Schultz, Phys. Rev. Lett. **84**, 4184 (2000).
[7] K. Aydin, K. Guven, M. Kafesaki, L. Zhang, C. M. Soukoulis, and E. Ozbay, Opt. Lett. **29**, 2623 (2004).
[8] R. Shelby, D. R. Smith, and S. Schultz, Science **292**, 77 (2001).
[9] N. Katsarakis, T. Koschny, M. Kafesaki, E. N. Economou, E. Ozbay, and C. M. Soukoulis, Phys. Rev. B **70**, 201101(R) (2004).
[10] E. Ozbay, Zh. Li, and K. Aydin, J. Phys.: Condens. Matter **20**, 304216 (2008).
[11] K. Aydin, Zh. Li, L. Sahin, and E. Ozbay, Opt. Express **16**, 8835 (2008); E. Ozbay and K. Aydin, Photonics Nanostruct. Fundam. Appl. **6**, 108 (2008).
[12] W. J. Padilla, D. N. Basov, and D. R. Smith, Mater. Today **9**, 28 (2006).
[13] D. R. Smith, J. B. Pendry, and M. C. K. Wiltshire, Science **305**, 788 (2004).
[14] T. J. Yen, W. J. Padilla, N. Fang, D. C. Vier, D. R. Smith, J. B. Pendry, D. N. Basov, and X. Zhang, Science **303**, 1494 (2004).
[15] N. Katsarakis, G. Konstantinidis, A. Kostopoulos, R. S. Penciu, T. F. Gundogdu, M. Kafesaki, E. N. Economou, Th. Koschny, and C. M. Soukoulis, Opt. Lett. **30**, 1348 (2005).
[16] G. Dolling, Ch. Enkrich, M. Wegener, C. M. Soukoulis, and S. Linden, Opt. Lett. **31**, 1800 (2006).
[17] Sh. Xiao, U. K. Chettiar, A. V. Kildishev, V. P. Drachev, and V. M. Shalaev, Opt. Lett. **34**, 3478 (2009).
[18] C. M. Soukoulis, S. Linden, and M. Wegener, Science **315**, 47 (2007).
[19] V. M. Shalaev, Nat. Photonics **1**, 41 (2007).
[20] W. Cai and V. Shalaev, *Optical Metamaterials: Fundamentals and Applications* (Springer, Dordrecht, 2009).
[21] J. B. Pendry, A. Holden, D. Robbins, and W. Stewart, IEEE Trans. Microwave Theory Tech. **47**, 2075 (1999).
[22] J. B. Pendry, A. J. Holden, W. J. Stewart, and I. Youngs, Phys. Rev. Lett. **76**, 4773 (1996); J. B. Pendry, A. J. Holden, D. J. Robbins, and W. J. Stewart, J. Phys.: Condens. Matter **10**, 4785 (1998).
[23] V. A. Podolskiy, A. K. Sarychev, and V. M. Shalaev, Opt. Express **11**, 735 (2003).
[24] V. M. Shalaev, W. Cai, U. K. Chettiar, H.-K. Yuan, A. K. Sarychev, V. P. Drachev, and A. V. Kildishev, Opt. Lett. **30**, 3356

(2005).
[25] G. Dolling, C. Enkrich, M. Wegener, S. Linden, J. Zhou, and C. M. Soukoulis, Opt. Lett. **30**, 3198 (2005).
[26] J. Zhou, E. N. Economou, Th. Koschny, and C. M. Soukoulis, Opt. Lett. **31**, 3620 (2006).
[27] S. Zhang, W. Fan, N. C. Panoiu, K. J. Malloy, R. M. Osgood, and S. R. J. Brueck, Phys. Rev. Lett. **95**, 137404 (2005); S. Zhang, W. Fan, B. K. Minhas, A. Frauenglass, K. J. Malloy, and S. R. J. Brueck, *ibid.* **94**, 037402 (2005).
[28] R. Ulrich, Infrared Phys. **7**, 37 (1967).
[29] M. Kafesaki, I. Tsiapa, N. Katsarakis, Th. Koschny, C. M. Soukoulis, and E. N. Economou, Phys. Rev. B **75**, 235114 (2007).
[30] C. Helgert, C. Menzel, C. Rockstuhl, E. P. Severin, E. B. Kley, A. Chipouline, A. Tunnermann, F. Lederer, and T. Pertsch, Opt. Lett. **34**, 704 (2009).
[31] C. Rockstuhl, Ch. Menzel, Th. Paul, Th. Pertsch, and F. Lederer, Phys. Rev. B **78**, 155102 (2008).
[32] U. K. Chettiar, A. V. Kildishev, H.-K. Yuan, W. Cai, S. Xiao, V. P. Drachev, and V. M. Shalaev, Opt. Lett. **32**, 1671 (2007).
[33] G. Dolling, M. Wegener, C. M. Soukoulis, and S. Linden, Opt. Lett. **32**, 53 (2007).
[34] N. Liu, H. Liu, S. Zhu, and H. Giessen, Nat. Photonics **3**, 157 (2009).
[35] G. Dolling, M. Wegener, and S. Linden, Opt. Lett. **32**, 551 (2007).
[36] J. Valentine, S. Zhang, Th. Zentgraf, E. Ulin-Avila, D. A. Genov, G. Bartal, and X. Zhang, Nature (London) **455**, 376 (2008).
[37] J. Zhou, Th. Koschny, M. Kafesaki, E. N. Economou, J. B. Pendry, and C. M. Soukoulis, Phys. Rev. Lett. **95**, 223902 (2005).
[38] S. Tretyakov, Metamaterials **1**, 40 (2007).
[39] A. Ishikawa, T. Tanaka, and S. Kawata, J. Opt. Soc. Am. B **24**, 510 (2007).
[40] A. K. Sarychev, G. Shvets, and V. M. Shalaev, Phys. Rev. E **73**, 036609 (2006).
[41] E. N. Economou, C. M. Soukoulis, and M. Kafesaki, J. Comput. Theor. Nanosci. **6**, 1827 (2009).
[42] C. M. Soukoulis, T. Koschny, J. Zhou, M. Kafesaki, and E. N. Economou, Phys. Status Solidi B **244**, 1181 (2007).
[43] L. Solymar, *Lectures on Electromagnetic Theory* (Oxford University Press, Oxford, 1976).
[44] D. R. Smith, S. Schultz, P. Markos, and C. M. Soukoulis, Phys. Rev. B **65**, 195104 (2002).
[45] D. R. Smith, D. C. Vier, Th. Koschny, and C. M. Soukoulis, Phys. Rev. E **71**, 036617 (2005).
[46] With this approach we omit the effect of the interaction among neighboring unit cells along propagation direction. This omission though does not alter the scaling response of our structures and the conclusion of the paper. Note that the main results of the interaction between neighboring unit cells along propagation direction (if this interaction is not very strong) is a shift in the resonance frequency and a broadening in the negative permeability regime.
[47] C. L. Holloway, A. Dienstfrey, E. F. Kuester, J. F. O'Hara, A. K. Azad, and A. J. Taylor, Metamaterials **3**, 100 (2009).
[48] C. Menzel, Th. Paul, C. Rockstuhl, T. Pertsch, S. Tretyakov, and F. Lederer, Phys. Rev. B **81**, 035320 (2010).
[49] C. R. Simovski and S. A. Tretyakov, Phys. Rev. B **75**, 195111 (2007).
[50] Th. Koschny, P. Markos, E. N. Economou, D. R. Smith, D. C. Vier, and C. M. Soukoulis, Phys. Rev. B **71**, 245105 (2005).
[51] M. W. Klein, C. Enkrich, M. Wegener, C. M. Soukoulis, and S. Linden, Opt. Lett. **31**, 1259 (2006).
[52] P. R. West, S. Ishii, G. Naik, N. Emani, V. M. Shalaev, and A. Boltasseva, Laser Photonics Rev. (to be published).
[53] Usually in simulations concerning realistic structures the factor γ employed is slightly larger than that of the bulk metal to account for the surface scattering effects.